Evaluation of a CD13 and Integrin $\alpha_v\beta_3$ Dual-Receptor Targeted Tracer ^{68}Ga-NGR-RGD for Ovarian Tumor Imaging: Comparison With ^{18}F-FDG

Yu Long[1,2], Fuqiang Shao[1,2], Hao Ji[1,2], Xiangming Song[1,2], Xiaoying Lv[1,2], Xiaotian Xia[1,2], Qingyao Liu[1,2], Yongxue Zhang[1,2], Dexing Zeng[3], Xiaoli Lan[1,2]* and Yongkang Gai[1,2]*

[1] Department of Nuclear Medicine, Union Hospital, Tongji Medical College, Huazhong University of Science and Technology, Wuhan, China, [2] Hubei Province Key Laboratory of Molecular Imaging, Wuhan, China, [3] Department of Radiology, University of Pittsburgh, Pittsburgh, PA, United States

Ovarian cancer has the highest mortality rate of gynecologic malignancy. ^{18}F-FDG positron emission tomography (PET) adds an important superiority over traditional anatomic imaging modalities in oncological imaging but has drawbacks including false negative results at the early stage of ovarian cancer, and false positives when inflammatory comorbidities are present. Aminopeptidase N (APN, also known as CD13) and integrin $\alpha_v\beta_3$ are two important targets overexpressed on tumor neo-vessels and frequently on ovarian cancerous cells. In this study, we used subcutaneous and metastatic models of ovarian cancer and muscular inflammation models to identify ^{68}Ga-NGR-RGD, a heterodimeric tracer consisting of NGR and RGD peptides targeting CD13 and integrin $\alpha_v\beta_3$, respectively, and compared it with ^{18}F-FDG. We found that ^{68}Ga-NGR-RGD showed greater contrast in SKOV3 and ES-2 tumors than ^{18}F-FDG. Low accumulation of ^{68}Ga-NGR-RGD but avid uptake of ^{18}F-FDG were observed in inflammatory muscle. In abdominal metastasis models, PET imaging with ^{68}Ga-NGR-RGD allowed for rapid and clear delineation of both peritoneal and liver metastases (3-6 mm), whereas, ^{18}F-FDG could not distinguish the metastasis lesions due to the relatively low metabolic activity in tumors and the interference of intestinal physiological ^{18}F-FDG uptake. Due to the high tumor-targeting efficacy, low inflammatory uptake, and higher tumor-to-background ratios compared to that of ^{18}F-FDG, ^{68}Ga-NGR-RGD presents a promising imaging agent for diagnosis, staging, and follow-up of ovarian tumors.

Keywords: positron emission tomography (PET), ovarian cancer, CD13, integrin $\alpha_v\beta_3$, dual-receptor targeted

INTRODUCTION

Ovarian cancer has the highest mortality rate of all gynecologic malignant cancers, with more than 80% of patients presenting with advanced disease (1). Due to their silent nature of the disease, patients often present with advanced stages at first diagnosis, which will result in 29-75% of patients succumbing to ovarian cancer within 5 years. However, if diagnosed at stage I (ovary defined), the

5-year survival rate exceeds 90% (1, 2). Therefore, it's a research priority to improve early detection and prevention, as a better prognosis correlated with early stage at diagnosis.

Functional imaging plays an essential role in the management of ovarian cancers. In particular, with the development and promotion of PET/MRI (3, 4) with excellent soft tissue contrast and digital PET scanner (5, 6) with higher sensitivity and diagnostic performance than analog PET, functional imaging will reduce radiation dose, enhance the diagnostic confidence and ensure the better strategies for patient management and personalized treatment, showing a wider clinical application prospect. ^{18}F-FDG positron emission tomography/computed tomography (PET/CT) imaging, as the most frequently used functional imaging method in oncological imaging, adds an important superiority over traditional anatomic imaging modalities by providing functional information about cellular glucose metabolism. However, ^{18}F-FDG PET is not recommended for the primary detection of ovarian cancers with a relatively low level of sensitivity (52-58%) and specificity (76-78%) (1, 7, 8), which might be due to tumor size and cystic or mucinous histological features with no/low metabolic activity in tumors (9, 10). Besides, it is limited by several pitfalls, such as higher ovarian glucose metabolism during menstruation and midcycle, physiologic accumulation in several benign diseases, as well as its imprecise distinction between cancerous growths and acute inflammation lesions (11–14). Novel PET agents targeting biological tumor features, including cell proliferation, angiogenesis, hypoxia, metabolism, and receptor overexpression, are pursued in preclinical researches to better detect early malignant lesions, evaluate the heterogeneity of biological features, and monitoring treatment response more accurately (10, 15–19).

Angiogenesis plays a prominent role in tumor growth, invasion and metastasis by providing abundant oxygen, nutrients, and metastatic conduits (20). aminopeptidase N (APN, also known as CD13) and integrin $\alpha_v\beta_3$ are two key regulators involved in tumor angiogenesis and tumor progression. They are overexpressed on the tumoral neo-endothelial cells during angiogenesis as well as cancerous cells, regarded as two important hallmarks of tumor angiogenesis (21–24). There are several studies have focused on the imaging and/or treatment of ovarian tumors by targeting CD13 (25, 26) or integrin $\alpha_v\beta_3$ (27, 28). However, these angiogenesis-related factors, including CD13 and integrin $\alpha_v\beta_3$, are usually differentially expressed in ovarian tumor tissues and cell lines due to the heterogeneity and genetically instability of the disease (29, 30), making it a very challenging approach to find "the optimal target", and may also be one of the reasons for drug resistance of cancer to monotherapy. Therefore, an alternative approach is to develop a complementary receptor-targeting agent for the detection and treatment of tumors.

Previously, we developed a CD13 and integrin $\alpha_v\beta_3$ dual-receptor targeted radiotracer, ^{68}Ga-NGR-RGD, which demonstrated promising results in PET imaging of breast cancers with superior imaging efficacy than monomeric ^{68}Ga-NGR and ^{68}Ga-RGD (31). Furthermore, the physiological uptake of ^{68}Ga-NGR-RGD is low in most normal organs, except kidneys, which may make this dual-receptor targeted tracer supplement or even be superior to ^{18}F-FDG PET/CT in the

early diagnosis and staging of ovarian tumors. In this study, we aim to evaluate the value of ^{68}Ga-NGR-RGD in PET/CT imaging of ovarian tumors. In addition, we also investigated its potential application in distinguishing tumors and inflammation. Routine ^{18}F-FDG imaging was also conducted as a control group in all prepared mice models.

MATERIALS AND METHODS

Synthesis of NGR-RGD and Radiolabeling
NGR-RGD was synthesized and radiolabeled using our previously developed method (31). Briefly, 150 μL sodium acetate buffer (0.25 M, pH 6.8) and 2 μL NGR-RGD (2 mM) were added to the tube containing 500 μL ^{68}GaCl$_3$ in 0.05 M HCl (150-200 MBq) and mixed. The final pH of the radiolabeling solution was approximately 4.0. Then, the mixture was heated at 95°C for 5 min. The radiolabeling field of the product ^{68}Ga-NGR-RGD was determined by radio-HPLC. ^{68}Ga was produced with a ^{68}Ge/^{68}Ga generator (Isotope Technologies Garching GmbH, Garching, Germany). Peptides were obtained commercially from Chinapeptide (Shanghai, China) or Gl Biochem (Shanghai, China).

Cell Culture
Human ovarian cancer cells, SKOV3, ES-2, and OVCAR4 were derived from our own laboratory preservation and cultured in GibcoDulbecco's Modified Eagle Medium/Nutrient mixture F-12 (DMEM/F12; Gibco, Carlsbad CA, USA), supplemented with 10% fetal bovine serum (FBS; Sciencell, Carlsbad CA, USA), 100 mg/mL streptomycin and 100 mg/mL penicillin (Solarbio, Shanghai, China) at 37°C in a humidified incubator with 5% CO_2.

Western Blot Analysis
Cancer cells were harvested, and total protein concentration was measured with the BCA protein assay kit (Aidlab, Beijing, China). After denaturation and separation by SDS-PAGE, proteins were transferred to a polyvinylidenefluoride (PVDF) membrane. Next, the blots were incubated with primary antibodies (1:500 anti-CD13, 1:1000 anti-Integrin alpha V, and 1:1000 anti-Integrin beta 3; Abcam, Cambridge MA, USA), and Glyceraldehyde-3-phosphate dehydrogenase (1:10000 GAPDH; Sungene, Tianjin, China). Next, the membrane was incubated with goat anti-rabbit IgG/HRP (diluted 1:20000; Sungene, Tianjin, China). The membrane was scanned by enhanced chemiluminescence (ECL kit, Beyotime) and analyzed using Quantity One software (Bio-Rad, Hercules CA, USA).

In Vitro Cell Uptake and Blocking Studies
Cells in logarithmic phase were harvested and counted using a cytometer (Cellmeter Mini, Nexcelom Bioscience LLC, Lawrence MA, USA). Cells were seeded in a 24-well plate at 2×10^5 cells per well 24 h in advance. 74 kBq ^{68}Ga-NGR-RGD in 50 μL PBS were added to each well and incubated at 37°C for 30 min, 1 h and 2 h. For blocking study, cells were pretreated with one hundred times

excess of non-radioactive NGR-RGD or NGR + RGD 15 min in advance. At the end of each time point, supernatant was collected, and cells were washed twice with pre-cooled PBS (wash 1) before lysed with 1 N sodium hydroxide; then each well was washed twice with pre-cooled PBS (wash 2). Cells, supernatant and wash solutions were subjected to radioactivity analysis using an automatic gamma counter (2470 WIZARD; PerkinElmer, Waltham MA, USA). The percentage of radioactivity taken up by the cells was calculated according to Equation 1, wherein Cpm represents decay-corrected radioactivity counts per minute.

$$\% \, radioactivity \, uptake = \\ [Cpm(Cells) + Cpm(Wash\,2)]/[Cpm(Cells) + Cpm(Supernatant) + Cpm(Wash\,1) + Cpm(Wash\,2)] \times 100$$

(Equation 1)

Animal Models

All animal studies were carried out according to the regulations and standards of the Institutional Animal Care and Use Committee of Tongji Medical College of Huazhong University of Science and Technology. Subcutaneous SKOV3 or ES-2 tumors were engrafted into 4-6 weeks-old female BALB/C nude mice obtained from Beijing HFK Bioscience Co. Ltd (Beijing, China). For implantation, 5×10^6 cancer cells in 100 μL PBS were subcutaneously injected into the right shoulder of each mouse. The mice were subjected to the following experiments when tumor size reached 8-10 mm. For mouse muscular inflammation models, 20 μL turpentine oil (Aladdin, China) was injected into the right thigh muscle of each mouse using a 29-gauge hypodermic needle. Turpentine oil caused visible redness and swelling within 3 h after injection and the inflammation mice were subjected to PET/CT scans at 24 h after injection of turpentine oil.

For abdominal metastasis models, SKOV3 or ES-2 cells were harvested and resuspended in a mixed solution (50% Matrigel, Corning and 50% PBS). Next, 5×10^6 tumor cells in 200 μL were injected into intra-peritoneal cavity (1, 32, 33). About 20 days later, the mice underwent PET/CT imaging.

Animal PET/CT Imaging and Biodistribution

PET/CT imaging was performed on the lnliView-3000B small animal PET/SPECT/CT (Novel Medical, Beijing, China). Overnight fasted tumor-bearing and inflammation mice received intravenous (i.v.) injection of 2.4-3 MBq ^{18}F-FDG. Animals were then returned to anesthesia induction box and subsequently anesthetized with 2.0% isoflurane delivered in 100% air. PET/CT scans were performed at 1 h after injection. The day after ^{18}F-FDG imaging, the PET/CT-based protocol for ^{68}Ga-NGR-RGD imaging were conducted, including intravenous injection of the ^{68}Ga-NGR-RGD solution (4-5.5 MBq) and identical procedures. For abdominal metastasis groups, PET/CT were performed at 1 h p.i. of ^{18}F-FDG or ^{68}Ga-NGR-RGD. Images were quantified via region-of-interest (ROI) analysis.

Following the terminal PET/CT scan, mice were sacrificed, and organs of interest were harvested, weighed, and γ-counted (2470 WIZARD; PerkinElmer, Waltham MA, USA) to validate the imaging data. The tracer accumulation of tissues and organs were noted by the percentage of injected dose per gram of tissue and corrected for radioactive decay (%ID/g).

Immunohistochemistry Analysis

Tumors were extracted, fixed in 4% paraformaldehyde, and then dehydrated and embedded in paraffin. Fixed tumor tissue sections (5 μm) were deparaffinized, rehydrated and permeabilized in EDTA buffer (pH 9.0). The sections were blocked for nonspecific binding by adding 3% hydrogen peroxide and 10% normal goat serum. Sections were incubated with primary antibodies at 4°C overnight (anti-$\alpha_v\beta_3$, 1:100; anti-CD13, 1:100; anti-CD31, 1:2000, Abcam, Cambridge MA, USA). Then sections were further stained with secondary antibody (HRP-labeled goat anti-rabbit IgG, diluted 1:50) at room temperature for 25 min, and then incubated with 3,3'-diaminobenzidine (DAB, Beyotime, Hangzhou, China) for 5 min. Last, slides were counterstained with hematoxylin (Beyotime), dehydrated, covered, and observed under light microscopy.

Statistical Analysis

Quantitative data were described as the mean ± standard deviation (SD). Statistical analysis was performed using student t-test and p-values < 0.05 were considered statistically significant.

RESULTS

CD13 and Integrin $\alpha_v\beta_3$ Expression in Ovarian Tumor Cell Lines

Expression levels of CD13 and integrin $\alpha_v\beta_3$ in three ovarian tumor cell lines were determined via Western blot, with GAPDH used as an internal control (**Figures 1A, B**). Strong integrin $\alpha_v\beta_3$ band intensity was observed in SKOV3 and OVCAR4 cell lines and strong CD13 staining was found in ES-2 cell line, indicating the high expression of CD13 and/or integrin $\alpha_v\beta_3$ in ovarian tumor cell lines.

Uptake Profile of ^{68}Ga-NGR-RGD in Ovarian Tumor Cells

To demonstrate the specificity of NGR-RGD for ovarian tumor cells, we conducted the cell uptake and blocking studies of ^{68}Ga-NGR-RGD in SKOV3, OVCAR4, and ES-2 ovarian tumor cells. High uptake of ^{68}Ga-NGR-RGD was observed in these three ovarian tumor cells with a gradually increasing trend over time (**Figure 1C**). On the contrary, minimal uptake of ^{68}Ga-NGR-RGD by SKOV3 and ES-2 cells was detected when pretreated with excess amounts of non-radiolabeled NGR-RGD or NGR+RGD (**Figure 1D**).

PET/CT Imaging and Biodistribution of ^{68}Ga-NGR-RGD in Subcutaneous Tumors

Next, we performed the PET/CT scan in SKOV3 and ES-2 tumor-bearing mice and turpentine oil-induced muscular inflammation mice using ^{18}F-FDG and ^{68}Ga-NGR-RGD. As
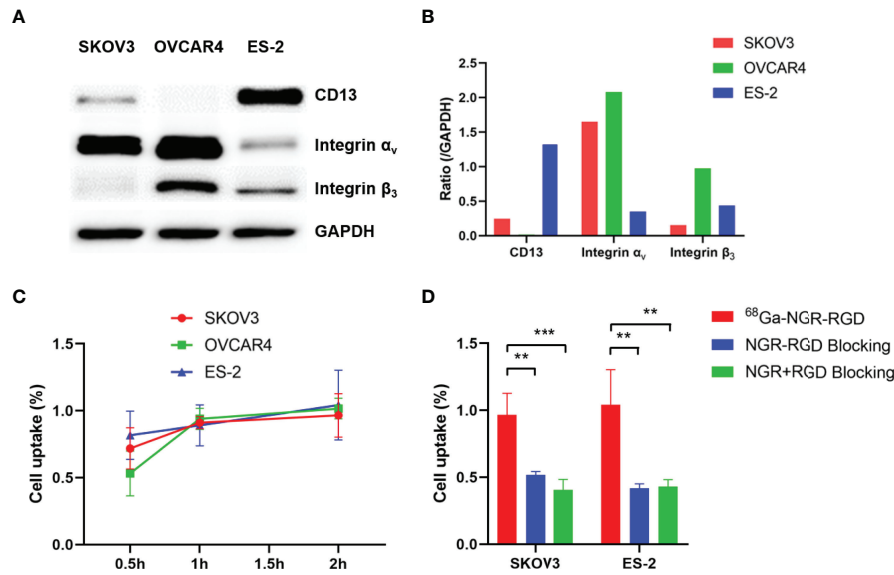
FIGURE 1 | Evaluation of binding affinity of 68Ga-NGR-RGD to ovarian tumor cells. **(A)** Western blot analysis of expression of CD13, integrin α_v and integrin β_3 in three ovarian tumor cell lines, with GAPDH used as internal control. **(B)** The semi-quantitative analysis was conducted through the integrated optical density ratio of CD13, integrin α_v and integrin β_3 to GAPDH. **(C)** Uptake of 68Ga-NGR-RGD in SKOV3, OVCAR4 and ES-2 ovarian tumor cell lines at 0.5 h, 1 h, 2 h. **(D)** Uptake of 68Ga-NGR-RGD in SKOV3 and ES-2 cells with or without blocking dose of NGR-RGD or NRG + RGD at 2 h. Cell uptake and blocking assays showed the 68Ga-NGR-RGD displayed specific binding to ovarian tumor cell lines. **p < 0.01, ***p < 0.001. Data are expressed as mean ± SD (n = 4).

shown in **Figure 2A**, 68Ga-NGR-RGD clearly delineated both SKOV3 and ES-2 ovarian tumors, and the tumor contrast of 68Ga-NGR-RGD PET imaging was greater than that of 18F-FDG. On the contrary, the uptake of 68Ga-NGR-RGD in inflammatory muscle was minimal, while avid uptake of 18F-FDG in them was observed.

The quantitative data were obtained from the region-of-interest (ROI) analysis. Consistent with the PET images, 68Ga-NGR-RGD showed significantly higher tumor-to-muscle (T/M) and tumor-to-liver (T/L) ratios, with values of 2.71 ± 0.21 and 1.05 ± 0.04 for SKOV3-bearing mice and 2.78 ± 0.34 and 1.43 ± 0.16 for ES-2-bearing mice (n=4; all p<0.05), as compared to low T/M and T/L ratios of 18F-FDG (0.92 ± 0.22 and 0.92 ± 0.04 for SKOV3, 1.03 ± 0.47 and 0.97 ± 0.26 for ES-2) (**Figures 2B, C**). We also quantified the tracer uptakes in inflammatory muscles and compared them with tumors. The uptakes of 68Ga-NGR-RGD in inflammatory muscles were much lower than tumors; however, their 18F-FDG uptakes were much higher (**Figure 2D**). And as expected, the tumor-to-inflammatory muscle ratios of 68Ga-NGR-RGD in SKOV3 and ES-2 were significantly higher than that of 18F-FDG (all p<0.001) (**Figure 2E**).

Biodistribution studies of 68Ga-NGR-RGD were conducted at 1 h post injection to validate the PET analysis. 68Ga-NGR-RGD uptake in SKOV3 and ES-2 xenografts were 0.68 ± 0.03%ID/g and 0.70 ± 0.17%ID/g, respectively (**Figure 3A**). And high tumor-to-muscle and tumor-to-liver ratios were recorded in both ovarian tumors (**Figure 3B**), consistent with PET imaging studies, further indicating the utility of 68Ga-NGR-RGD in the diagnosis of ovarian cancer.

Immunohistochemistry Staining in Tumor Tissues

SKOV3 tumor sections showed high expression of integrin $\alpha_v\beta_3$ and moderate CD13, and ES-2 tumor sections showed abundant CD13 and moderate integrin $\alpha_v\beta_3$ (**Figure 3C**). The staining of endothelial marker CD31 (cluster of differentiation 31) was also conducted to evaluate the angiogenesis of tumors. Both SKOV3 and ES-2 tumors displayed neovascularity. Immunohistochemical results of tumor tissues were consistent with western blot results.

PET Imaging and Biodistribution in Metastatic Models

To further investigate the potential application of 68Ga-NGR-RGD in detecting metastases, SKOV3 and ES-2 abdominal metastatic models were established by injecting tumor cells intraperitoneally to simulate peritoneum implantation metastasis of ovarian cancers. As shown in **Figure 4**, peritoneal metastases could be easily delineated from 68Ga-NGR-RGD PET/CT imaging in both ovarian tumor models. However, 18F-FDG PET showed limited value in detecting these metastatic lesions, which was limited by the relatively low uptake in tumors and high background signals. In the images of 68Ga-NGR-RGD (**Figures 4A, C**), several focal uptakes were found in the abdominal space of both SKOV3 and ES-2 group mice, suspected to be the peritoneal implantations; while in the images of 18F-FDG (**Figures 4B, D**), several strips with high signal were observed in abdomen. Surgical explorations were done on the same mice after scanning, finding reddish-white
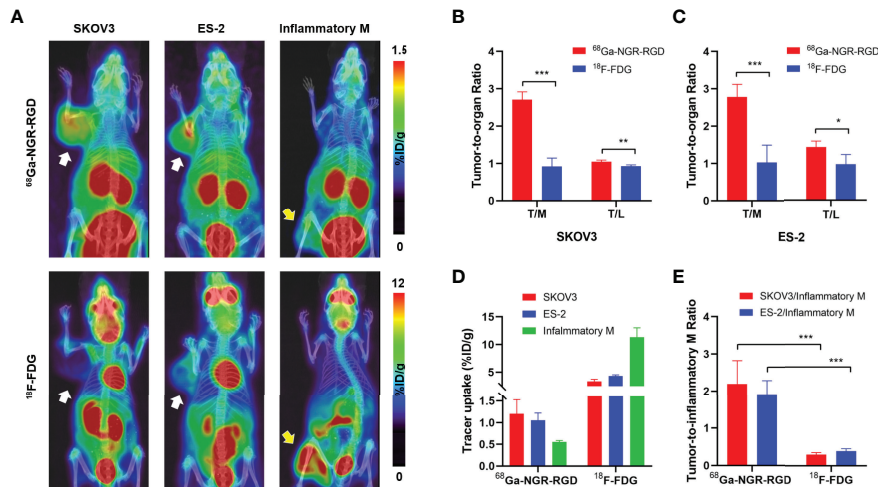
FIGURE 2 | PET/CT imaging and quantitative analysis of ^{68}Ga-NGR-RGD and ^{18}F-FDG in subcutaneous ovarian cancer models and inflammation models. **(A)** Representative static small PET/CT images of ^{68}Ga-NGR-RGD and ^{18}F-FDG in SKOV3 and ES-2 xenograft mice and turpentine oil-induced muscular inflammation mice at 1 h post radiotracer injection. White arrows indicated tumors and yellow arrows indicate the inflammatory muscles. **(B, C)** Tumor-to-muscle (T/M) and tumor-to-liver (T/L) ratios among ^{68}Ga-NGR-RGD and ^{18}F-FDG imaging in SKOV3 **(B)** and ES-2 **(C)** xenograft mice. **(D)** Quantification of ^{68}Ga-NGR-RGD and ^{18}F-FDG uptake in SKOV3 and ES-2 tumors and inflammatory muscle. **(E)** Tumor-to-inflammatory muscle (Tumor/Inflammatory M) ratios. *p < 0.05, **p < 0.01, ***p < 0.001. Data are expressed as mean ± SD (n = 4).

nodules with a slightly firm texture in all these groups (**Supplementary Figure 2**). The nodules were extracted for further evaluation, along with muscle, large intestine, small intestine, spleen, and kidney. The nodular tissues (3-6 mm) were confirmed to be ^{68}Ga-NGR-RGD-avid but ^{18}F-FDG-nonavid by ex-vivo PET imaging. High radioactivity accumulation was found in kidney, indicating that the tracer was mainly excreted *via* kidney. Other tissues in the abdominal cavity such as intestines and spleens showed low signals, indicating that the high signal focuses in PET images were the tumor metastases; whereas, uptake of ^{18}F-FDG was high in large intestine, suggesting the high signal regions in the image were not metastases but intestinal physiological uptake. Additionally, there were some liver metastases found in ES-2 abdominal models (**Figure 4E**). The liver metastases of ovarian tumor showed a strong uptake of ^{68}Ga-NGR-RGD but a similar low uptake of ^{18}F-FDG as healthy liver, which further demonstrated that ^{68}Ga-NGR-RGD has excellent metastasis detection efficiency of small peritoneal implants and liver metastases over ^{18}F-FDG. The hematoxylin-eosin (HE) staining confirmed that the lesions on the liver were metastatic tumors (**Figure 4F**).

Ex-vivo biodistribution studies showed 2.11 ± 0.67%ID/g and 0.97 ± 0.23%ID/g tumor uptake of ^{68}Ga-NGR-RGD in the SKOV3 and ES-2 abdominal metastasis models, respectively (**Figure 5** and **Supplementary Table 1**). Tumor uptakes of SKOV3 metastases were higher than SKOV3 subcutaneous tumors, which might be attributed to a better blood supply and the smaller metastasis size (34). Higher tumor-to-muscle (T/M) and tumor-to-liver (T/L) ratios were recorded in ^{68}Ga-NGR-RGD group, consistent with the results of s.c. tumor models (**Supplementary Figure 3**). More specifically, tumor-to-small

intestine (T/SI) and tumor-to-large intestine (T/LI) ratios of ^{68}Ga-NGR-RGD in abdominal metastasis models were significantly higher than that of ^{18}F-FDG (p<0.01), which was consistent with PET imaging (**Figure 5C**).

DISCUSSION

CD13 and integrin $\alpha_v\beta_3$ are two important angiogenic factors involved in the regulation of tumor angiogenesis and tumor progression and several related targeted tracers were developed for the detection of ovarian cancers, with proven specific and sensitive targeting ability to ovarian cancers (22–25). However, due to the high heterogeneity, and genetical instability of ovarian cancer leading to a progressive increase in the number of different angiogenic factors as the cancer progress to advanced stages (20, 29, 30, 35, 36), the single-receptor targeted imaging strategies may only cover a limited subset of the patients. Owing to the dual-receptor binding property, improved *in vivo* kinetics, and increased circulation half-life, heterodimer tracers are expected to be more sensitive than single receptor-targeted tracers, especially when only one receptor type is overexpressed in a tumor model (31, 37, 38). In this study, we investigated the ability and potential of our recently developed dual CD13 and integrin $\alpha_v\beta_3$ targeted tracer ^{68}Ga-NGR-RGD, as a tumor-specific PET imaging agent, for the early diagnosis and staging of ovarian tumors. ^{68}Ga-NGR-RGD exhibited sharp contrasts in subcutaneous ovarian xenografts and metastases, higher tumor-to-background ratios, and in addition, high capability for distinguishing tumor from inflammatory tissue which is
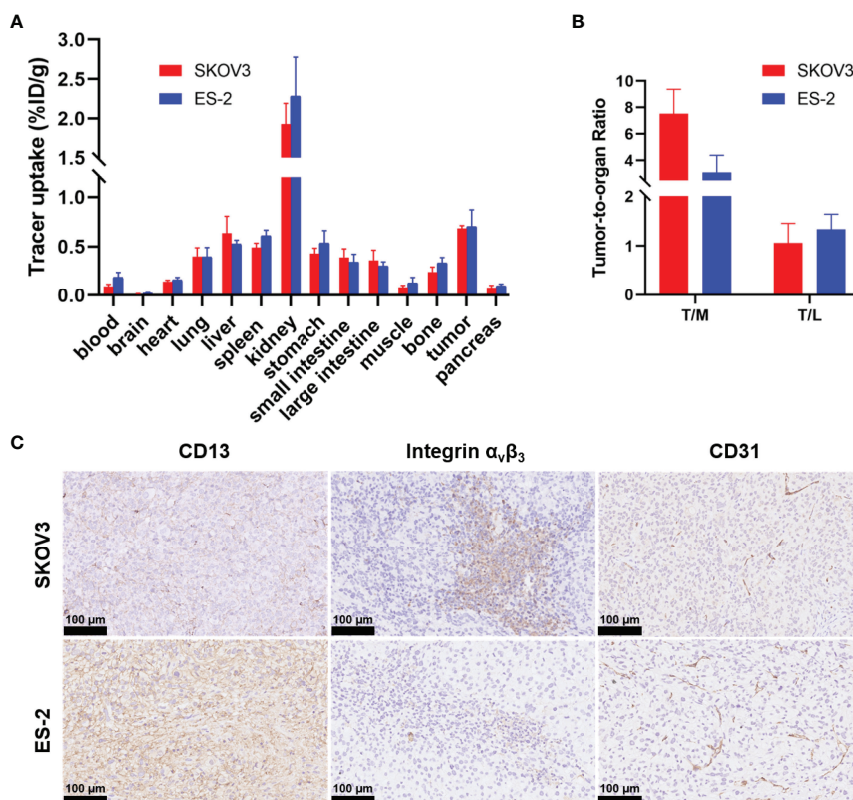
FIGURE 3 | Biodistribution data of ^{68}Ga-NGR-RGD in ovarian xenograft mice and immunohistochemistry analysis of tumor tissue sections. (A) Biodistribution of ^{68}Ga-NGR-RGD in SKOV3 and ES-2 subcutaneous ovarian tumor models at 1 h after injection (n = 4). (B) Tumor-to-muscle (T/M) and tumor-to-liver (T/L) ratios of ^{68}Ga-NGR-RGD in SKOV3 and ES-2 xenograft mice. (C) Immunohistochemistry staining of CD13, integrin $\alpha_v\beta_3$ and CD31 in SKOV3 and ES-2 tumor sections. Scale bar = 50 μm.

superior to ^{18}F-FDG, suggesting it has great potential to provide an enhancement to the standard diagnostic imaging of ovarian cancer.

Here, three ovarian tumor cell lines were selected and confirmed to express high level of integrin $\alpha_v\beta_3$ and/or CD13, indicating the possibility of dual-receptor targeted tracer for the detection of ovarian tumors. *In vitro* studies showed high uptake of ^{68}Ga-NGR-RGD in three ovarian cancer cell lines, and blocking studies showed significant decrease tracer uptake, validating the specific binding of our radio-tracer towards integrin $\alpha_v\beta_3$ and CD13 on ovarian tumor cells. Both SKOV3 and ES-2 subcutaneous metastatic tumors were clearly visualized by ^{68}Ga-NGR-RGD PET imaging at 1 h post tracer injection, although SKOV3 cells expressed a high level of integrin $\alpha_v\beta_3$ but relatively low level of CD13, and ES-2 expressed a high level of CD13 but low integrin $\alpha_v\beta_3$. These PET imaging results suggested a broad application of ^{68}Ga-NGR-RGD in the detection of ovarian tumors with improved tumor-targeting efficacy and sensitivity. Specifically, we could readily identify the location of small peritoneal implants and liver metastases (3-6 mm) in SKOV3 and ES-2 abdominal metastatic models. These results demonstrated the utility of ^{68}Ga-NGR-RGD for the sensitive detection of integrin $\alpha_v\beta_3$ and/or CD13 positive ovarian tumors.

When compared with ^{18}F-FDG, greater contrast of subcutaneous and metastatic tumors was observed in ^{68}Ga-NGR-RGD PET imaging of SKOV3 and ES-2 ovarian tumor models with significantly higher tumor-to-background ratios (T/M and T/L). In addition, the overall abdominal background uptake of ^{68}Ga-NGR-RGD with exception of urinary system was relatively low, so small metastases could be clearly delineated and easily differentiated from background uptake of surrounding tissues. However, ^{18}F-FDG accumulated heavily in the large intestine due to physiological intestinal uptake, which often makes it difficult to distinguish between normal intestinal uptake with adjacent abdominal or pelvic tumor or nodal uptake (39–42). Moreover, in turpentine oil-induced muscular inflammatory lesions (**Supplementary Figure 1**), high uptake of ^{18}F-FDG was observed in inflammatory cells (neutrophils and macrophages) and granulation tissues, which showed similar histology and FDG-avid features to the reported studies (43–45), mimicking a false-positive lesion of ^{18}F-FDG PET. In contrast to ^{18}F-FDG, ^{68}Ga-NGR-RGD showed low accumulation in inflammatory muscles. Therefore, the false-positive results in physical uptake of surrounding tissues and inflammatory changes detected by ^{18}F-FDG can potentially be avoided using ^{68}Ga-NGR-RGD as a more tumor-specific imaging agent.
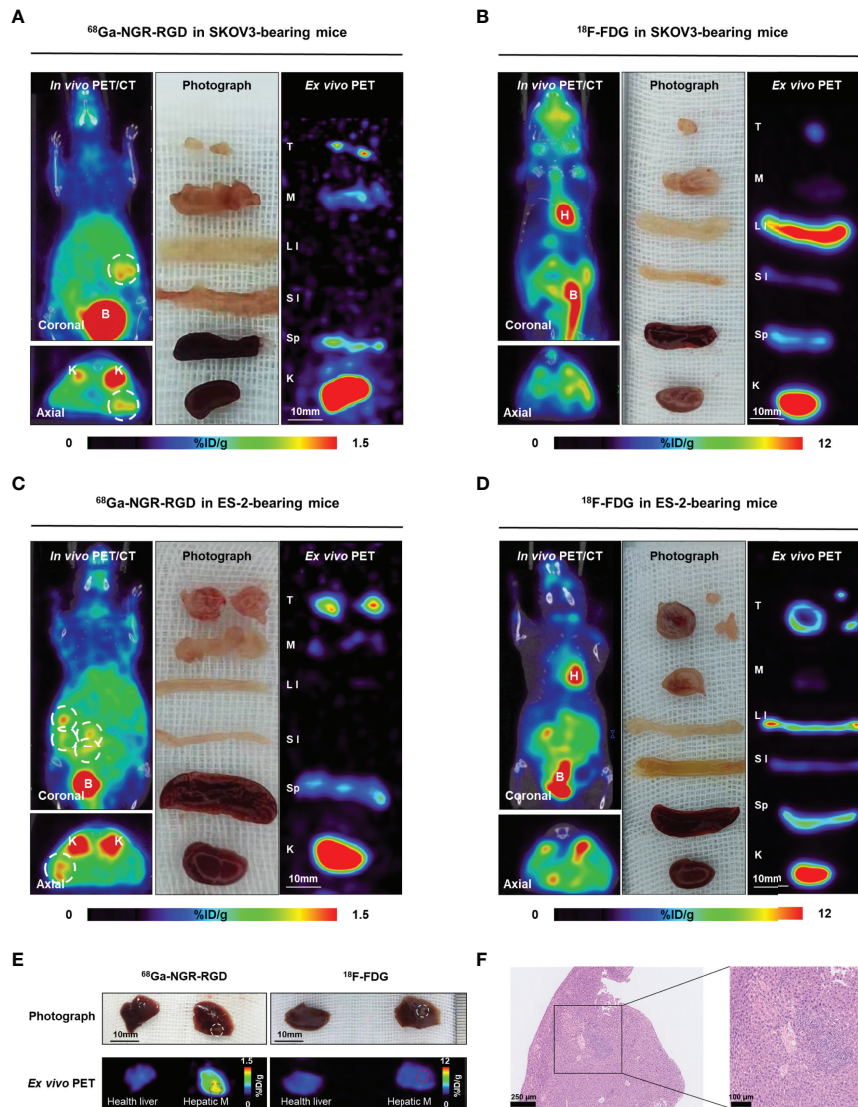
FIGURE 4 | Radiological-surgical correlation of abdominal metastatic models. **(A–D)** Representative static PET/CT images of 68Ga-NGR-RGD and 18F-FDG in SKOV3 and ES-2 abdominal ovarian metastasis models at 1 h post injection. In 68Ga-NGR-RGD PET/CT imaging, several metastatic lesions with strong uptake were found in the peritoneal space [**(A, C)**, white circle]. In 18F-FDG PET/CT imaging, there were several stripe high uptake foci **(B, D)**. Surgical exploration was done in the same animal after PET/CT imaging. Diffuse reddish-white nodules with a slightly firm texture were seen in the peritoneal space. Ex vivo PET imaging of excised tissues was performed. The small metastases showed relatively high 68Ga-NGR-RGD uptake and low 18F-FDG uptake. H, heart; B, bladder; T, tumor; M, muscle; LI, large intestine; SI, small intestine; Sp, spleen; K, kidney. Scale bar = 10 mm **(E)** ES-2 hepatic metastases (Hepatic M) showed strong uptake of 68Ga-NGR-RGD, but a similar low uptake of 18F-FDG as healthy liver. **(F)** HE staining confirmed that the lesion on liver was tumor tissue. Scale bar = 250 μm or 100 μm.

There are many potential applications that probably profit from PET imaging targeting CD13 and integrin $\alpha_v\beta_3$. With the great contrast of small tumors and higher tumor-to-background ratios than 18F-FDG, 68Ga-NGR-RGD could provide significant additional information, such as the relationship between tumor lesions with adjacent tissues and distant metastases, for determining TNM staging and optimal treatment options, so it suggests that 68Ga-NGR-RGD is a potential candidate to be added to the workup and treatment planning of patients with ovarian tumors. In addition, anti-angiogenesis therapy has been regarded as a new

era for tumor treatment in recent years, and targeting the tumor neovascularization, including CD13 and integrin $\alpha_v\beta_3$, has become a widely accepted therapeutic strategy in clinic (46, 47). The heterodimer strategy may also help with the development of therapy molecules, allowing for selection of responders and treatment response monitoring during and after therapy.

One limitation of this study is that only two types of tumor models were used, while ovarian tumors are highly heterogeneous with complex tumor components (48). Future work will evaluate tumor uptake of 68Ga-NGR-RGD in other types of tumor models,
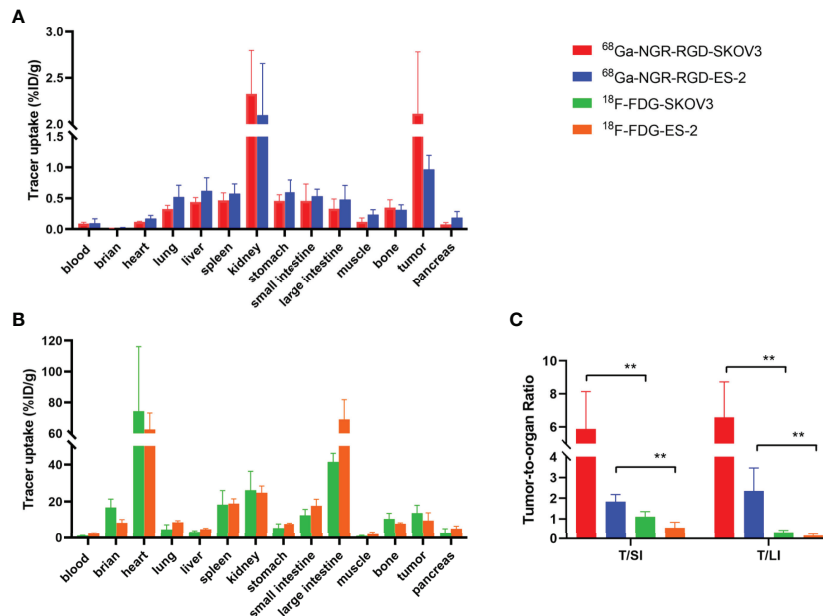
FIGURE 5 | Biodistribution for the validation of PET/CT results. Biodistribution of ^{68}Ga-NGR-RGD in SKOV3 and ES-2 **(A)** abdominal metastatic ovarian tumor models and ^{18}F-FDG in SKOV3 and ES-2 **(B)** metastatic models at 1 h after tracer injection. **(C)** Metastatic tumor lesions showed avid ^{68}Ga-NGR-RGD uptake with a significantly higher tumor-to-small intestine (T/SI) and tumor-to-large intestine (T/LI) comparing to ^{18}F-FDG. **p < 0.01. Data are expressed as mean ± SD (n = 4).

especially patient-derived xenograft models, with a various expression of CD13 and integrin $\alpha_v\beta_3$. Currently, ^{68}Ga is usually produced by an in-house ^{68}Ge/^{68}Ga generator, and one elution could provide a dose enough for 2–5 patients based on the specification of the generator. Therefore, we believe the final cost of a ^{68}Ga-tracer scan will be acceptable and should be close to routine ^{18}F-FDG PET scans (after considering the cyclotron and its maintenance). Clinical studies evaluating the safety and efficacy of the dual-receptor targeted tracer in humans are ongoing, which will be free of charge for the patients enrolled, and we will report relevant data in the future.

In conclusion, ^{68}Ga-NGR-RGD demonstrated a promising application for early diagnosis, staging, and follow-up of ovarian cancer, as it showed high tracer uptake, sharp contrasts in subcutaneous xenograft and metastases, and higher tumor-to-background ratios in ovarian tumor models with different expression levels of CD13 and integrin $\alpha_v\beta_3$, demonstrating superior diagnostic values than ^{18}F-FDG PET/CT. Meanwhile, *in vivo* PET imaging studies showed significantly lower accumulation of ^{68}Ga-NGR-RGD in inflammatory lesions as compared to ^{18}F-FDG, suggesting the potential of ^{68}Ga-NGR-RGD for differentiating between tumor and non-tumor inflammation.

DATA AVAILABILITY STATEMENT

The original contributions presented in the study are included in the article/**Supplementary Material**. Further inquiries can be directed to the corresponding authors.

ETHICS STATEMENT

The animal study was reviewed and approved by the Institutional Animal Care and Use Committee of Tongji Medical College of Huazhong University of Science and Technology.

AUTHOR CONTRIBUTIONS

YL wrote the majority of the manuscript. YL, FS, and HJ performed the canine operations. XS and XYL assisted in PET imaging and biodistribution studies. XX, QL, and YZ provided specific experimental advice and technique support. YG and DZ was the primary developer of NGR-RGD and provided guidance for dosing and imaging decisions. YL, XLL, and YG designed the experiments, analyzed the data, and edited the manuscript. All authors contributed to the article and approved the submitted version.

SUPPLEMENTARY MATERIAL

The Supplementary Material for this article can be found online at: https://www.frontiersin.org/articles/10.3389/fonc.2022.884554/full#supplementary-material

REFERENCES

1. Siegel RL, Miller KD, Jemal A. Cancer Statistics, 2019. *CA Cancer J Clin* (2019) 69:7–34. doi: 10.3322/caac.21551

2. Iyer VR, Lee SI. MRI, CT, and PET/CT for Ovarian Cancer Detection and Adnexal Lesion Characterization. *AJR Am J Roentgenol* (2010) 194:311–21. doi: 10.2214/AJR.09.3522

3. Beiderwellen K, Grueneisen J, Ruhlmann V, Buderath P, Aktas B, Heusch P, et al. [(18)F]Fdg PET/MRI vs. PET/CT for Whole-Body Staging in Patients With Recurrent Malignancies of the Female Pelvis: Initial Results. *Eur J Nucl Med Mol Imaging* (2015) 42:56–65. doi: 10.1007/s00259-014-2902-8

4. Khiewvan B, Torigian DA, Emamzadehfard S, Paydary K, Salavati A, Houshmand S, et al. An Update on the Role of PET/CT and PET/MRI in Ovarian Cancer. *Eur J Nucl Med Mol Imaging* (2017) 44:1079–91. doi: 10.1007/s00259-017-3638-z

5. López-Mora DA, Carrió I, Flotats A. Digital PET vs Analog Pet: Clinical Implications. *Semin Nucl Med* (2021) 52:302–11. doi: 10.1053/j.semnuclmed.2021.10.004

6. Alberts I, Prenosil G, Sachpekidis C, Weitzel T, Shi K, Rominger A, et al. Digital Versus Analogue PET in [(68)Ga]Ga-PSMA-11 PET/CT for Recurrent Prostate Cancer: A Matched-Pair Comparison. *Eur J Nucl Med Mol Imagl* (2020) 47:614–23. doi: 10.1007/s00259-019-04630-y

7. Fenchel S, Grab D, Nuessle K, Kotzerke J, Rieber A, Kreienberg R, et al. Asymptomatic Adnexal Masses: Correlation of FDG PET and Histopathologic Findings. *Radiology* (2002) 223:780–8. doi: 10.1148/radiol.2233001850

8. Rieber A, Nüssle K, Stöhr I, Grab D, Fenchel S, Kreienberg R, et al. Preoperative Diagnosis of Ovarian Tumors With MR Imaging: Comparison With Transvaginal Sonography, Positron Emission Tomography, and Histologic Findings. *AJR Am J Roentgenol* (2001) 177:123–9. doi: 10.2214/ajr.177.1.1770123

9. Rockall AG, Cross S, Flanagan S, Moore E, Avril N. The Role of FDG-PET/CT in Gynaecological Cancers. *Cancer Imaging* (2012) 12:49–65. doi: 10.1102/1470-7330.2012.0007

10. Ponisio MR, Dehdashti F. A Role of PET Agents Beyond FDG in Gynecology. *Semin Nucl Med* (2019) 49:501–11. doi: 10.1053/j.semnuclmed.2019.06.008

11. Lerman H, Metser U, Grisaru D, Fishman A, Lievshitz G, Even-Sapir E. Normal and Abnormal 18f-FDG Endometrial and Ovarian Uptake in Pre- and Postmenopausal Patients: Assessment by PET/Ct. *J Nucl Med* (2004) 45:266–71.

12. Rahman WT, Wale DJ, Viglianti BL, Townsend DM, Manganaro MS, Gross MD, et al. The Impact of Infection and Inflammation in Oncologic (18)F-FDG PET/CT Imaging. *BioMed Pharmacot* (2019) 117:109168. doi: 10.1016/j.biopha.2019.109168

13. Almuhaideb A, Papathanasiou N, Bomanji J. 18f-Fdg PET/CT Imaging in Oncology. *Ann Saudi Med* (2011) 31:3–13. doi: 10.4103/0256-4947.75771

14. Boré P, Descourt R, Ollivier L, Le Roux PY, Abgral R. False Positive 18f-Fdg Positron Emission Tomography Findings in Schwannoma-A Caution for Reporting Physicians. *Front Med (Lausanne)* (2018) 5:275. doi: 10.3389/fmed.2018.00275

15. Boyle AJ, Tong J, Zoghbi SS, Pike VW, Innis RB, Vasdev N. Repurposing (11) C-PS13 for PET Imaging of Cyclooxygenase-1 in Ovarian Cancer Xenograft Mouse Models. *J Nucl Med* (2021) 62:665–8. doi: 10.2967/jnumed.120.249367

16. Sanduleanu S, Wiel A, Lieverse R, Marcus D, Ibrahim A, Primakov S, et al. Hypoxia PET Imaging With [18f]-HX4-A Promising Next-Generation Tracer. *Cancers (Basel)* (2020) 12:1322. doi: 10.3390/cancers12051322

17. Trencsényi G, Márián T, Lajtos I, Krasznai Z, Balkay L, Emri M, et al. 18fdg, [18f] FLT, [18f]FAZA, and 11C-Methionine Are Suitable Tracers for the Diagnosis and *In Vivo* Follow-Up of the Efficacy of Chemotherapy by miniPET in Both Multidrug Resistant and Sensitive Human Gynecologic Tumor Xenografts. *BioMed Res Int* (2014) 2014:787365. doi: 10.1155/2014/787365

18. Makvandi M, Pantel A, Schwartz L, Schubert E, Xu K, Hsieh CJ, et al. A PET Imaging Agent for Evaluating PARP-1 Expression in Ovarian Cancer. *J Clin Invest* (2018) 128:2116–26. doi: 10.1172/JCI97992

19. Matsumoto H, Watabe T, Igarashi C, Tachibana T, Hihara F, Waki A, et al. Evaluation of (64)Cu-Labeled New Anti-Egfr Antibody NCAB001 With Intraperitoneal Injection for Early Pet Diagnosis of Pancreatic Cancer in Orthotopic Tumor-Xenografted Mice and Nonhuman Primates. *Pharmaceut (Basel)* (2021) 14:950. doi: 10.3390/ph14100950

20. Lugano R, Ramachandran M, Dimberg A. Tumor Angiogenesis: Causes, Consequences, Challenges and Opportunities. *Cell Mol Life Sci* (2020) 77:1745–70. doi: 10.1007/s00018-019-03351-7

21. Luan Y, Xu W. The Structure and Main Functions of Aminopeptidase N. *Curr Med Chem* (2007) 14:639–47. doi: 10.2174/092986707780059571

22. Hashida H, Takabayashi A, Kanai M, Adachi M, Kondo K, Kohno N, et al. Aminopeptidase N Is Involved in Cell Motility and Angiogenesis: Its Clinical Significance in Human Colon Cancer. *Gastroenterology* (2002) 122:376–86. doi: 10.1053/gast.2002.31095

23. Danhier F, Le Breton A, Préat V. RGD-Based Strategies to Target Alpha(V) Beta(3) Integrin in Cancer Therapy and Diagnosis. *Mol Pharm* (2012) 9:2961–73. doi: 10.1021/mp3002733

24. Kumar CC. Integrin Alpha V Beta 3 as a Therapeutic Target for Blocking Tumor-Induced Angiogenesis. *Curr Drug Targets* (2003) 4:123–31. doi: 10.2174/1389450033346830

25. Cui SX, Qu XJ, Gao ZH, Zhang YS, Zhang XF, Zhao CR, et al. Targeting Aminopeptidase N (APN/CD13) With Cyclic-Imide Peptidomimetics Derivative CIP-13f Inhibits the Growth of Human Ovarian Carcinoma Cells. *Cancer Lett* (2010) 292:153–62. doi: 10.1016/j.canlet.2009.11.021

26. Yang Y, Zhang J, Zou H, Shen Y, Deng S, Wu Y. Synthesis and Evaluation of (68) Ga-Labeled Dimeric cNGR Peptide for PET Imaging of CD13 Expression With Ovarian Cancer Xenograft. *J Cancer* (2021) 12:244–52. doi: 10.7150/jca.49628

27. Jin ZH, Tsuji AB, Degardin M, Sugyo A, Obara S, Wakizaka H, et al. Radiotheranostic Agent (64)Cu-Cyclam-RAFT-C(-RGDfK-)(4) for Management of Peritoneal Metastasis in Ovarian Cancer. *Clin Cancer Res* (2020) 26:6230–41. doi: 10.1158/1078-0432.CCR-20-1205

28. Minamimoto R, Karam A, Jamali M, Barkhodari A, Gambhir SS, Dorigo O, et al. Pilot Prospective Evaluation of (18)F-FPPRGD2 PET/CT in Patients With Cervical and Ovarian Cancer. *Eur J Nucl Med Mol Imaging* (2016) 43:1047–55. doi: 10.1007/s00259-015-3263-7

29. Kobayashi M, Sawada K, Kimura T. Potential of Integrin Inhibitors for Treating Ovarian Cancer: A Literature Review. *Cancers (Basel)* (2017) 9:83. doi: 10.3390/cancers9070083

30. Friedman R. Drug Resistance in Cancer: Molecular Evolution and Compensatory Proliferation. *Oncotarget* (2016) 7:11746–55. doi: 10.18632/oncotarget.7459

31. Gai Y, Jiang Y, Long Y, Sun L, Liu Q, Qin C, et al. Evaluation of an Integrin α(V)β(3) and Aminopeptidase N Dual-Receptor Targeting Tracer for Breast Cancer Imaging. *Mol Pharm* (2020) 17:349–58. doi: 10.1021/acs.molpharmaceut.9b01134

32. Wu GJ, Zeng GF. METCAM/MUC18 is a Novel Tumor and Metastasis Suppressor for the Human Ovarian Cancer SKOV3 Cells. *BMC Cancer* (2016) 16:136. doi: 10.1186/s12885-016-2181-9

33. Wen W, Liang W, Wu J, Kowolik CM, Buettner R, Scuto A, et al. Targeting JAK1/STAT3 Signaling Suppresses Tumor Progression and Metastasis in a Peritoneal Model of Human Ovarian Cancer. *Mol Cancer Ther* (2014) 13:3037–48. doi: 10.1158/1535-7163.MCT-14-0077

34. Soret M, Bacharach SL, Buvat I. Partial-Volume Effect in PET Tumor Imaging. *J Nucl Med* (2007) 48:932–45. doi: 10.2967/jnumed.106.035774

35. Wang Z, Dabrosin C, Yin X, Fuster MM, Arreola A, Rathmell WK, et al. Broad Targeting of Angiogenesis for Cancer Prevention and Therapy. *Semin Cancer Biol* (2015) 35 Suppl:S224–224S243. doi: 10.1016/j.semcancer.2015.01.001

36. Kroeger PT Jr, Drapkin R. Pathogenesis and Heterogeneity of Ovarian Cancer. *Curr Opin Obstet Gynecol* (2017) 29:26–34. doi: 10.1097/GCO.0000000000000340

37. Liu Z, Niu G, Wang F, Chen X. (68)Ga-Labeled NOTA-RGD-BBN Peptide for Dual Integrin and GRPR-Targeted Tumor Imaging. *Eur J Nucl Med Mol Imaging* (2009) 36:1483–94. doi: 10.1007/s00259-009-1123-z

38. Judmann B, Braun D, Wängler B, Schirrmacher R, Fricker G, Wängler C. Current State of Radiolabeled Heterobivalent Peptidic Ligands in Tumor Imaging and Therapy. *Pharmaceut (Basel)* (2020) 13:173. doi: 10.3390/ph13080173

39. Franquet E, Palmer MR, Gifford AE, Selen DJ, Chen YC, Sedora-Roman N, et al. Rifaximin Suppresses Background Intestinal 18f-FDG Uptake on PET/CT Scans. *Nucl Med Commun* (2014) 35:1026–31. doi: 10.1097/MNM.0000000000000170

40. Gutman F, Alberini JL, Wartski M, Vilain D, Le Stanc E, Sarandi F, et al. Incidental Colonic Focal Lesions Detected by FDG Pet/Ct. *AJR Am J Roentgenol* (2005) 185:495–500. doi: 10.2214/ajr.185.2.01850495

41. Heusner TA, Hahn S, Hamami ME, Kim UH, Baumeister R, Forsting M, et al. Gastrointestinal 18f-FDG Accumulation on PET Without a Corresponding CT Abnormality Is Not an Early Indicator of Cancer Development. *Eur Radiol* (2009) 19:2171–9. doi: 10.1007/s00330-009-1405-7

42. Tatlidil R, Jadvar H, Bading JR, Conti PS. Incidental Colonic Fluorodeoxyglucose Uptake: Correlation With Colonoscopic and Histopathologic Findings. *Radiology* (2002) 224:783–7. doi: 10.1148/radiol.2243011214

43. Watabe T, Ikeda H, Nagamori S, Wiriyasermkul P, Tanaka Y, Naka S, et al. (18)F-FBPA as a Tumor-Specific Probe of L-Type Amino Acid Transporter 1 (LAT1): A Comparison Study With (18)F-FDG and (11)C-Methionine Pet. *Eur J Nucl Med Mol Imaging* (2017) 44:321–31. doi: 10.1007/s00259-016-3487-1

44. Lee SJ, Thien Quach CH, Jung KH, Paik JY, Lee JH, Park JW, et al. Oxidized Low-Density Lipoprotein Stimulates Macrophage 18f-FDG Uptake *Via* Hypoxia-Inducible Factor-1α Activation Through Nox2-Dependent Reactive Oxygen Species Generation. *J Nucl Med* (2014) 55:1699–705. doi: 10.2967/jnumed.114.139428

45. Takeshita N, Tohma T, Miyauchi H, Suzuki K, Nishimori T, Ohira G, et al. Suture Granuloma With False-Positive Findings on FDG-PET/CT Resected *Via* Laparoscopic Surgery. *Int Surg* (2015) 100:604–7. doi: 10.9738/INTSURG-D-14-00140.1

46. He L, Zhu W, Chen Q, Yuan Y, Wang Y, Wang J, et al. Ovarian Cancer Cell-Secreted Exosomal miR-205 Promotes Metastasis by Inducing Angiogenesis. *Theranostics* (2019) 9:8206–20. doi: 10.7150/thno.37455

47. Ferrara N, Kerbel RS. Angiogenesis as a Therapeutic Target. *Nature* (2005) 438:967–74. doi: 10.1038/nature04483

48. Torre LA, Trabert B, DeSantis CE, Miller KD, Samimi G, Runowicz CD, et al. Ovarian Cancer Statistics, 2018. *CA Cancer J Clin* (2018) 68:284–96. doi: 10.3322/caac.21456

Conflict of Interest: The authors declare that the research was conducted in the absence of any commercial or financial relationships that could be construed as a potential conflict of interest.

Publisher's Note: All claims expressed in this article are solely those of the authors and do not necessarily represent those of their affiliated organizations, or those of the publisher, the editors and the reviewers. Any product that may be evaluated in this article, or claim that may be made by its manufacturer, is not guaranteed or endorsed by the publisher.